

HEXIT-SAT: a mission concept for X-ray grazing incidence telescopes from 0.5 to 70 keV

Fabrizio Fiore^a, Giuseppe C. Perola^b, Giovanni Pareschi^c, Oberto Citterio^c, Alberto Anselmi^d
and Andrea Comastri^e

^aINAF Osservatorio Astronomico di Roma, via Frascati 33, Monteporzio, Italy I00040

^bUniversita' Roma Tre, via della Vasca Navale 84, Roma, Italy I00100

^cINAF Osservatorio Astronomico di Brera, Via E. Bianchi 46, Merate (Lc), Italy I23807

^dAlenia Spazio, Strada Antica di Collegno 253, Torino, Italy I10146

^eINAF Osservatorio Astronomico di Bologna, via Ranzani 1, Bologna, Italy I40127

ABSTRACT

While the energy density of the Cosmic X-ray Background (CXB) provides a statistical estimate of the super massive black hole (SMBH) growth and mass density in the Universe, the lack, so far, of focusing instrument in the 20-60 keV (where the CXB energy density peaks), frustrates our effort to obtain a comprehensive picture of the SMBH evolutionary properties. HEXIT-SAT (High Energy X-ray Imaging Telescope SATellite) is a mission concept capable of exploring the hard X-ray sky with focusing/imaging instrumentation, to obtain an unbiased census of accreting SMBH up to the redshifts where galaxy formation peaks, and on extremely wide luminosity ranges. This will represent a leap forward comparable to that achieved in the soft X-rays by the Einstein Observatory in the late 70'. In addition to accreting SMBH, and very much like the Einstein Observatory, this mission would also have the capabilities of investigating almost any type of the celestial X-ray sources. HEXIT-SAT is based on high throughput ($>400 \text{ cm}^2 @ 30 \text{ keV}$; $> 1200 \text{ cm}^2 @ 1 \text{ keV}$), high quality (15 arcsec Half Power Diameter) multi-layer optics, coupled with focal plane detectors with high efficiency in the full 0.5-70keV range. Building on the BeppoSAX experience, a low-Earth, equatorial orbit, will assure a low and stable particle background, and thus an extremely good sensitivity for faint hard X-ray sources. At the flux limits of $1/10 \mu\text{Crab}$ (10-30 keV) and $1/3 \mu\text{Crab}$ (20-40 keV) (reachable in one Msec observation) we should detect ~ 100 and ~ 40 sources in the 15 arcmin FWHM Field of View respectively, thus resolving $> 80\%$ and $\sim 65\%$ of the CXB where its energy density peaks.

Keywords: Grazing incidence optics, Cosmic X-ray Background

1. INTRODUCTION

X-ray imaging observations, performed first by Einstein and ROSAT in the soft X-ray band below $\sim 3 \text{ keV}$ and then by ASCA, BeppoSAX, XMM-Newton and Chandra up to 8-10 keV, have increased by orders of magnitude the discovery space for both galaxies with an active nucleus and for thermal plasma sources. As an example, Fig. 1 shows a projection of the 2-10 keV discovery space for AGN in the redshift versus X-ray to optical flux ratio (X/O) plane. The use of collimated detectors on board the UHURU, Ariel-V, and HEAO1 satellites in the 1970 decade (filled circles in figure) led to the discovery of < 1000 X-ray sources in the whole sky, most of which with X/O in the range 1-10 and very few at $z > 0.5$. The first imaging detectors working above 2 keV on board ASCA and BeppoSAX produced the first systematic observations of AGN up to $z=2-3$, and resolved up to $1/4$ of the CXB below 10 keV. The superior image quality of Chandra and the high throughput of XMM-Newton expanded the discovery space even further, down to X/O as low as 10^{-3} , starting to probe the X-ray emission of star-forming galaxies, and, most important, up to X/O of several hundred, where many highly obscured, high luminosity type 2 QSO, and many high redshift QSO are found. This allowed us to study the accretion process on wide ranges of cosmic times, environments and accretion efficiencies, from very low power AGNs in luminous bulges (low X/O sources), to normal AGN (X/O=0.1-10), to highly obscured QSOs (X/O $\gtrsim 10$). The situation

F.F.: E-mail fiore@mporzio.astro.it

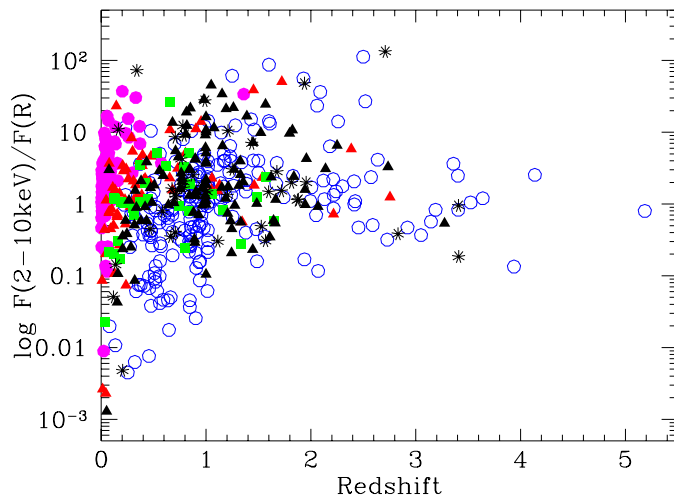


Figure 1. A projection of the 2-10 keV discovery space for AGN in the $z - X\text{-ray to optical flux ratio (X/O)}$ plane. HEAO1= Filled circles; BeppoSAX = filled triangles; ASCA = filled squares; XMM-Newton = stars; Chandra = open circles.

at energies just slightly higher than 8-10 keV contrasts startlingly with this picture. Above 10 keV the most sensitive observations have been performed so far by a collimated instruments, the BeppoSAX PDS¹ (see Fiore, Matt and Ghisellini contributions at the 2003 “Restless Universe” Symposium) and only a few hundred sources are known in the whole sky, a situation recalling the pre-Einstein era during the 70’. This limitation frustrates the possibility to investigate obscured sources (a column density of 10^{24} cm^{-2} produces an optical depth of 1 at 10 keV for solar abundances) and sources dominated by non-thermal emission. We clearly need to open up a new window in X-ray astronomy above 10 keV, producing an increase of the discovery space similar to that obtained with the first soft and medium X-ray imaging missions. This can be achieved today because the technology necessary to focus efficiently the hard X-rays is mature. Indeed, several proposals for an hard X-ray mission have been presented in the last years.²⁻⁵ The purpose of this paper is to help focusing better the science goals and the needed technological developments. As a result of this exercise, performed by a large number of people from the Italian astrophysical and industrial communities, the HEXIT-SAT mission concept was born. The main characteristics and architecture of this space project are also reported in this paper.

2. MAIN SCIENTIFIC MOTIVATION

One of the most challenging goals of modern cosmology is to understand how the structure of the Universe formed and how it evolved with time. Until ten years ago AGN, shining in about 1/100 of galaxies of the local Universe, were considered slightly more than a curiosity, in the framework of galaxy evolution. Indeed, the Cosmic background in X-rays is about 2 orders of magnitude less intense than that in the infrared and in the optical. Two seminal discoveries are now changing completely this view. The first is the discovery of SMBH in the center of most nearby bulge dominated galaxies: their masses are proportional to bulge properties like mass, luminosity, velocity dispersion and concentration^{6,7} The tightness and steepness of these correlations imply strong interplays and feedbacks between the nucleus and its host galaxy which in turn imply that if we want to fully understand galaxy formation and evolution we must understand the formation and growth of SMBH and AGN evolution. The second discovery is that the cosmic history of AGN activity depends on their luminosity: the number and luminosity density of both low and high luminosity AGN rises steeply from the local Universe up to $z \sim 1$ but then, while the density of high luminosity AGN stays constant, that of low luminosity AGN decreases toward higher redshifts.⁸⁻¹⁰ The combined behaviour is similar to that of the star-formation rate,^{9,11}

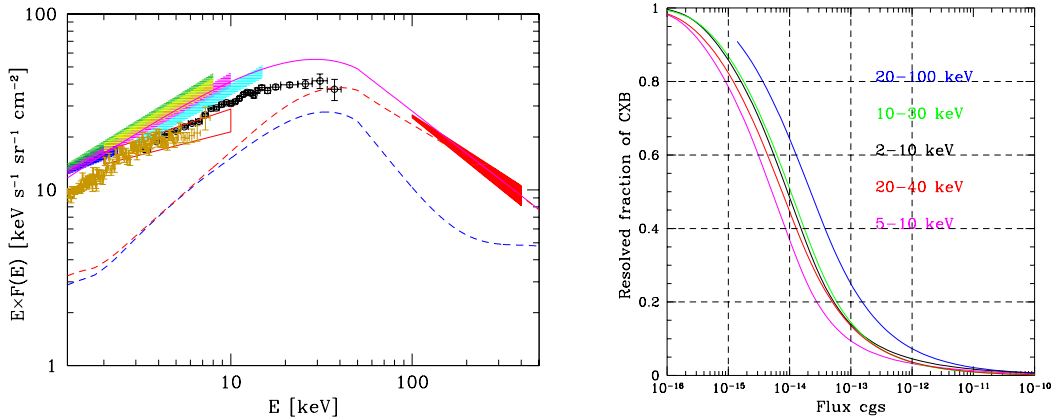


Figure 2. a), left panel: the residual CXB after subtraction of the fraction resolved below 10 keV, computed assuming a power law cutoff energy of 100 keV (upper dashed curve) and of 400 keV (lower dashed curve). b), right panel: the fraction of resolved CXB as a function of the flux computed using the Comastri model. Curves from top to bottom refer to the bands: 20-100 keV; 10-30 keV; 2-10 keV; 20-40 keV; 5-10 keV.

and indeed, most of the CXB is thought to be in place at $z < 2$.^{12,13} This redshift range ($z=1-2$) can then be considered as the “golden epoch of galaxy and AGN activity”. Conversely, hierarchical clustering Λ CDM models for the formation and evolution of galaxies predicts a number of low luminosity AGN much higher than observed by Chandra and XMM-Newton at $z \gtrsim 1$.¹³ This disagreement may be due to a selection effect, if highly obscured AGN are common at these redshifts (as in the nearby Universe) but are missed (or their luminosity is badly under-estimated) in Chandra and XMM-Newton surveys. Indeed, only 40–50% of the hard (7-10 keV) CXB has been resolved¹⁴ leaving room for a population of highly obscured AGN at $z \simeq 1 - 2$ where the bulk of the CXB is produced. The spectrum of the “unresolved” background can be estimated by subtracting from the total CXB (normalized to the De Luca & Molendi 2004 XMM-Newton determination¹⁵) the contribution of the sources detected by Chandra and XMM-Newton below 8-10 keV. This is given in Fig. 2a) adapted from Comastri 2004.¹⁶ Not surprisingly, this spectrum is reminiscent of that of extremely obscured sources. In conclusion, the light-up and evolution of obscured accreting SMBH is today still largely unknown. It is clear that for an unbiased census of the AGN population making the bulk of the CXB and in particular of highly obscured sources ($N_H \gtrsim 10^{24} \text{ cm}^{-2}$, sensitive observations extending up to about 70 keV are needed.

2.1. Additional scientific motivations

Besides the main goal described in the previous section, a mission with good sensitivity and imaging quality up to 60-70 keV would have the capability to investigate almost any type of the celestial X-ray sources, and, in particular it would be crucial for the study of hard X-ray non-thermal emission from a wide variety of sources. Acceleration mechanisms in AGN, cluster of galaxies and stellar sources (both single stars, binaries and Supernovae Remnants) are today rather poorly known and studied. In the following we give two examples of forefront science that could highly benefit from such a mission.

Thanks to the PDS sensitivity BeppoSAX was able for the first time to observe a few blazars in which the peak of the synchrotron emission reached around 100 keV (while the peak of the Inverse Compton (IC) component is in the GeV or even TeV range, the so called High Energy Peaked sources, HEP). These nearby low luminosity sources are probably the tip of the iceberg of a much larger population. The about 2 orders of magnitude increase in sensitivity achievable with respect to the PDS will make feasible both the discovery and the study of a statistical sample of HEP, and, possibly, the discovery of even more extreme sources, with the synchrotron peak at even higher energies.

The presence in cluster of galaxies of a diffuse component of relativistic particles is witnessed by the observation, in a several of them, of synchrotron diffuse radio emission (so called radio-halo sources). The inevitable IC interaction of the relativistic electrons with the photons of the cosmic microwave background should provide emission in the X-rays, whose intensity would dominate the thermal emission at $E > 10$ keV. Its detection would constrain at the same time the number of electrons and the strength of the magnetic field (not possible using the synchrotron emission alone). A positive result, but still controversial (a few σ), was obtained by the BeppoSAX PDS in the Coma cluster and in Abell 2256^{17,18} but also see.¹⁹ The much increased sensitivity available with focusing optics with respect to the PDS and, most important, their high quality imaging capabilities, will allow a detailed mapping of the IC component, and therefore of the intra-cluster magnetic field and relativistic particles.

2.2. Requirements

Fig. 2a) shows that the highly obscured sources contributing to the “unresolved” fraction of the CXB are probably still a minority population even in the 10-30 keV band, contributing to 40 – 50% of the total CXB in that band. In the 20-40 keV band the contribution of the highly obscured AGN undetected below 10 keV should be 50-70% of the total. This means that if we want to discover sizeable samples of this elusive population and make a fundamental step forward with respect to the Chandra and XMM-Newton results, we need to resolve in sources the majority of the 10-30 keV CXB, say 80%, similar to what Chandra and XMM-Newton did in the 2-10 keV band, and at least 50% of the 20-40 keV CXB. From Fig. 2b), showing the fraction of the CXB resolved in sources as a function of the flux in different energy bands calculated using the Comastri et al. AGN synthesis model of the CXB,¹² we see that the above goals can be reached if we can push the observations in the 10-30 keV band to 2×10^{-15} erg cm⁻² s⁻¹ (corresponding to $\sim 0.13 \mu\text{Crab}$) and to 7×10^{-15} erg cm⁻² s⁻¹ (corresponding to 3/4 of μCrab) in the 20-40 keV band.

2.2.1. Image quality and confusion limit

The goal flux limits in the previous section have been computed using the Comastri et al. prediction in the 10-30 keV and 20-40 keV bands. We verified that these prediction agree well with those obtained by Menci et al. (2004) using a completely different theoretical approach, and with those of Ueda et al. (2004) which extrapolate at harder energies the best fit to the observed 2-10 keV AGN luminosity function. Using all these predictions we evaluate in $\sim 2300 \text{deg}^{-2}$ and $\sim 350 \text{deg}^{-2}$ the source density at the flux limits of 1/10 and 3/4 μCrab . Using the standard criterion for source confusion we calculate the probability P to have two sources closer than the beam size as a function of the beam size θ_{FWHM} , assuming the higher source density. We find that Point Spread Functions (PSFs) with Half Power Diameter (HPD) of 15, 30 and 50 arcsec (and with $\text{HPD} = 2\theta_{FWHM}$, which is typical of realistic grazing incidence mirrors, because of the power lost in the broad scattering wings), give probabilities of 10%, 30% and 50% respectively. These should actually be considered as lower limits because the classical analytical formula of course does not account for the efficiency of the detection algorithm, the PSF sampling, and source clustering. This means that a mirror PSF with $\text{HPD} \lesssim 15 - 20$ is necessary to avoid strong source confusion ($P < 10 - 20\%$) at the flux limit of 0.1 μCrab .

3. OUTLINING A MISSION CONCEPT: THE PAYLOAD

3.1. Telescope design tradeoffs

A flux of 0.1 μCrab gives 0.057 counts/Msec/cm² in the 10-30 keV band and therefore an effective area of $\gtrsim 350$ cm² @30 keV is needed to collect 20 counts in 1Msec, which would give a 3σ detection assuming a similar background count rate. the mirror effective area is given by:

$$A_{eff} \sim FL^2 \times \theta^2 \times R^2$$

where FL is the telescope focal length, theta is the grazing angle and R is the mirror reflectivity. Therefore at least two strategies can be envisaged to obtain large collecting areas at high energy: a) very long focal lengths with usual single-layer reflecting coatings; b) high mirror reflectivity, which can be obtained using multilayer coatings on mirror shells with grazing incidence close to the critical angles that would be achieved for total reflection in the 10 20 keV energy band, e.g. 0.2-0.3 deg. For our exercise we followed the second strategy. An

important advantage in keeping not too high the focal length (less than 10 m) is a small focal spot (due to a more reduced plate-scale) with a consequent decrease of the intrinsic background counts. In addition, another fundamental advantage of this strategy is that sufficiently large reflection angles, as permitted by multilayer mirrors, allow one to obtain a still relatively large Field of View (FOV), of the order of 15 arcmin diameter FWHM. This is important because the source densities at the goal flux limits in the 10-30 keV and 20-40 keV bands are 120 and 12 sources per 15arcmin diameter FOV respectively.

3.2. The X-ray Mirror Modules

Number of modules	4
Number of nested mirror shells	50
Reflecting coating	200 bi-layers W/Si
Geometrical profile	Wolter I (lin. approx)
Focal Length	8000 mm
Total Shell Height	800 mm
Plate scale	26 arcsec/mm
Total Shell Height	800 mm
Material of the mirror walls	electroformed Ni
Min-Max Top Diameter	112 - 330 mm
Min - Max angle of incidence	0.096 - 0.295 deg
Min-Max wall thickness	0.120 - 0.350 mm
Total Mirror Weight (1 module)	95
Field-of-View (diameter FWHM)	15 arcmin
Single module effective area	75 cm ² @40 keV

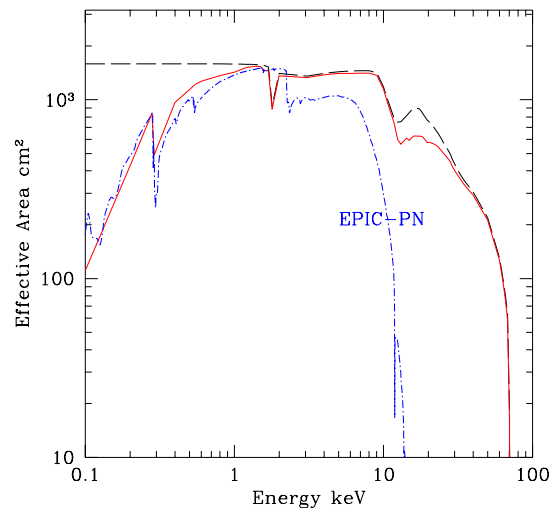


Figure 3. a), left panel: Table with the main characteristics of the HEXIT-SAT mirror modules. b), right panel: total effective area of 4 modules (long dashed line), effective area corrected for detector efficiency (solid line) compared with the EPIC-PN effective area (dot-dashed line).

The main characteristics of the mirror modules designed for HEXIT-SAT are given in Fig. 3a). The needed effective area is obtained using 4 mirror modules, each with 8m focal length. The sequence design for the thicknesses of bi-layers along the multilayer stacks will continuously change following a power-law, in agreement with the method adopted by.²⁰ The power-law parameters have been separately optimized for each mirror shell by a global mathematical approach (the so called "Iterated Simplex Algorithm" procedure), assuming as a figure of merit the enhancement of the effective area in an energy band as large as possible. The total on-axis effective area for 4 multilayer modules, not-corrected for the detector efficiencies, is reported in Fig. 3b). It should be noted that the cut-off of effective area around 70 keV is determined by the K absorption edge of W layers.

The fabrication technique for the hard X-ray mirrors is based on direct replication by Ni electroforming of the multi-layer film previously deposited onto a mandrel. This approach is an upgrade, after appropriate modifications, of the production process (developed in Italy) successfully used for the Au-coated high throughput optics with high quality imaging properties of the BeppoSAX,²¹ JET-X/SWIFT and XMM-Newton soft X-ray experiments. The study to produce a complete prototype has been financed by the Italian Space Agency (ASI) and is on going (Pareschi et al. this conference²²), with the goal of demonstrating the readiness and the quality of the technology. In particular, the manufacturing method adopted for the production of multi-layer optics foresees the following steps: a) a superpolished Aluminum mandrel with an external layer ($\sim 100 \mu\text{m}$ thick) of electroless Nickel (Kanigen) is fabricated. The shape of the mandrel is the negative profile of a linear-approximation Wolter I mirror to be realized. b) on the mandrel surface is then deposited a multi-layer film by means of a proper deposition technique, able to alternate the deposition of two different materials, in order to allow the growth of both materials (spacer and absorber) of the multi-layer stack. The mandrel is mounted with its axis of symmetry

perpendicular to the deposition beam of evaporated material and it is rotated during the deposition process. During the film growth the layer thickness is measured by means of a cooled Quartz microbalance, while the uniformity of the sputtering beam is obtained using an equalization mask; c) the mandrel is then put into an electrolytic bath, where a layer of Nickel is deposited on the multi-layer stack. Afterward the multi-layer mirror is separated from the mandrel by cooling it, exploiting the fact that the CTE of the Al (i.e., the bulk material of the mandrel) is about twice larger than the electroformed Ni walls. It should be noted that this approach has been already successfully proved for flats and small-dimension mandrels by using the Ion Beam Sputtering as a deposition method.²³ The process is now being up-graded with the use of the Ion assisted E-beam Deposition instead of Ion sputtering, which more easily permits to extend the use of the technique to large-size mandrels.

3.3. Focal plane detectors

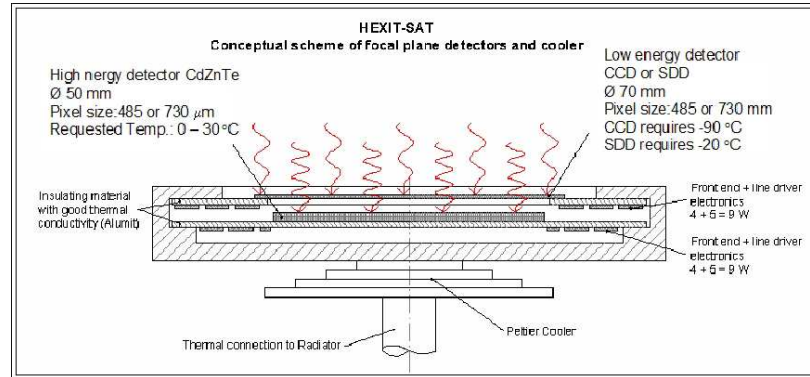


Figure 4. Conceptual scheme of focal plane detectors and cooler

The goal to be achieved is to have a detector system that matches well the optics performances over the broad 0.5 - 70 keV energy range. We need a small area imaging system that has both good spatial and energy resolution. The angular resolution of the X-ray telescope will be ~ 15 arcsec HPD, which requires, in the focal plane, a spatial resolution no larger than 0.2-0.3 mm, to sample the PSF at least with two pixels. The detector must also have good efficiency not only in the so called "hard" X-ray band ($\gtrsim 10$ keV) but also it is considered of extreme importance having an optimal response also in the "classical" X-ray band (0.5 - 10 keV), where the HEXIT-SAT telescopes present the largest effective area. We have therefore envisaged two possible solutions:

- i) the first one is based on the use of solid state detectors covering the 10-70 keV band, placed in series after a CCD or a SDD detector, which in turn can detect photons between 0.5 and 12 keV. This is the baseline solution adopted in this document for the sensitivity graphs and textual references 4. The hard X-ray detector choice will be a CdZnTe hybrid solid state detector (the possibility of using CdTe crystals is an alternative solution). CdZnTe detectors combine the room temperature operation with a good spectroscopic performance, theoretically approaching that of Ge and Si detectors (that, however, would require complex cryogenic systems). This clearly implies a saving in the overall instrumentation complexity, cost and weight. Due to the relatively high atomic numbers (49) and to the high density (6.1 g/cm^3), the quantum efficiency is also very good ($\sim 99\%$ for a 1 mm thick crystal @ 55 keV). Thanks to their low capacitance CdZnTe detectors allow to reach high energy resolution when an accurate coupling to custom front-end electronics is used. The required pixel size of 0.2-0.3mm implies further developments of the current CdZnTe pixelated detectors. The realization of a prototype detector is planned in the framework of the mentioned Pareschi et al. study (also see Del Sordo et al. 2004²⁴)
- ii) the other approach is instead based upon a SDD optically connected to an array of microscintillator crystals.²⁵

CCD detectors are readily available but require temperatures as low as -90C. Silicon drift chambers have very good energy resolution at higher temperature (-20C), but require some development.

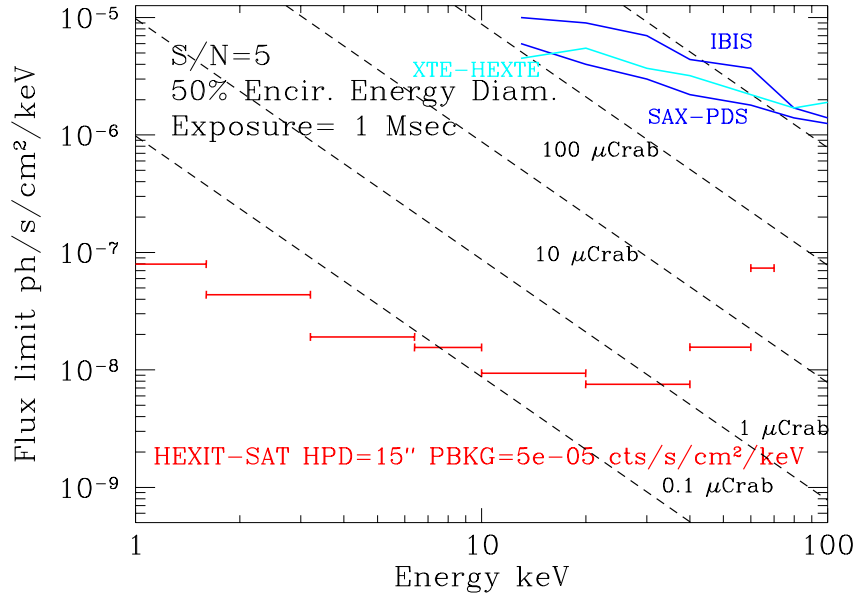


Figure 5. S/N=5 flux limit reachable in 1Msec in the 1-70 keV band

3.4. Expected performances

The design briefly illustrated in the previous section implies that the deepest HEXIT-SAT exposures will be background dominated. The ultimate performances of this experiment depend therefore on the satellite environment and on our ability to reject the different background components: a) particle background; b) X-ray photons produced by the interaction of the particle with the spacecraft; the CXB. The BeppoSAX PDS proved that one of the best environment is a low Earth orbit with low inclination, and therefore we will use this baseline orbit in the following calculations. The background seen in the BeppoSAX PDS NaI(Tl) detector, after active rejection in the CsI(Na) detector and in the lateral and top shields, is of $\sim 5 \times 10^{-5}$ cts/s/cm² per each mm of detector thickness. We assume this value as the reference particle induced background (direct particle + X-ray induced photons). Using the effective area in Fig. 3b), which also includes detector efficiency, and this internal background plus the contribution of the CXB, we computed the flux limits as a function of the energy in Fig. 5. Our mission design produces an improvement in sensitivity of a factor of ~ 300 with respect to the BeppoSAX PDS at 30 keV. Fig. 6 shows the flux limit (for a signal to noise of 3) as a function of the exposure time in the 10-30 keV and 20-40 keV bands. For the baseline background in 1 Msec we can reach a 10-30 keV flux of 1.4×10^{-15} erg cm⁻² s⁻¹ (0.09 μ Crab) and a 20-40 keV flux of 3.3×10^{-15} erg cm⁻² s⁻¹ (0.35 μ Crab). At this flux limits there should be ~ 120 and ~ 40 sources per FOV in the 2 bands respectively, which correspond to resolving $\gtrsim 80\%$ and $\sim 65\%$ of the 10-30 keV and 20-40 keV CXB, similar to the goals indicated in Sect. 2.2.

We tried to understand up to which redshift HEXIT-SAT is able to detect AGN similar to the highly obscured Seyfert galaxies common in the local Universe. Two examples are given in Fig. 7. We have redshifted the spectra of the low luminosity Seyfert 2 galaxy Circinus galaxy (distance of 4 Mpc, $\log L_{2-10keV} = 41.7$, $N_H = 2 \times 10^{24}$) and of the more luminous Seyfert 2 galaxy Markarian 3 ($z=0.0135$, $\log L_{2-10keV} = 43.8$, $N_H = 2 \times 10^{24}$) and compared with the 1 Msec flux limit of HEXIT-SAT. Objects similar to Markarian 3 are detectable up to $z \sim 1$, i.e. at the peak of the AGN number and luminosity density, while the low luminosity Circinus galaxy would be detected up to $z \sim 0.1$. We conclude that the proposed mission would produce a large increase of the discovery space for obscured AGN.

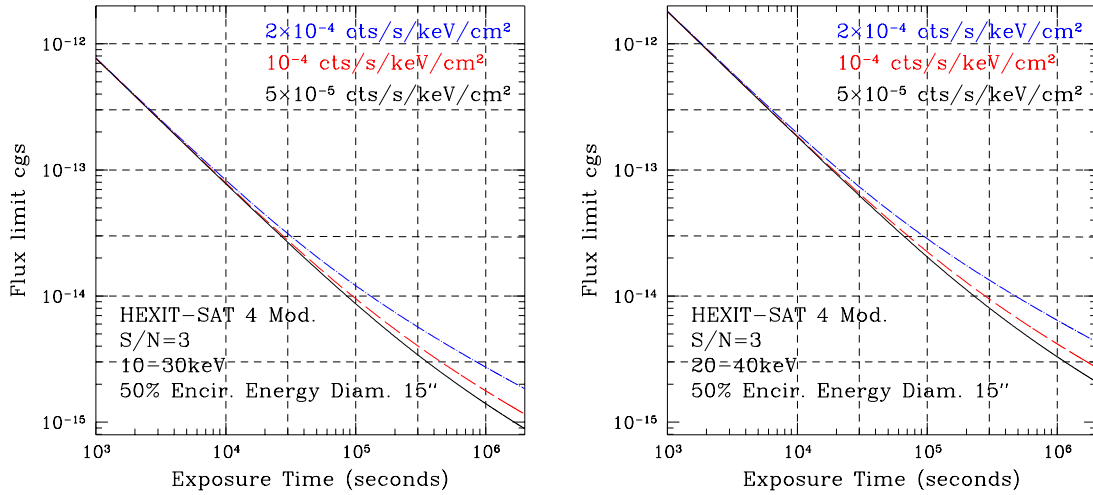


Figure 6. S/N=3 flux limits in the 10-30 keV (left panel) and 20-40 keV (right panel) as a function of the exposure time for three particle induced background values

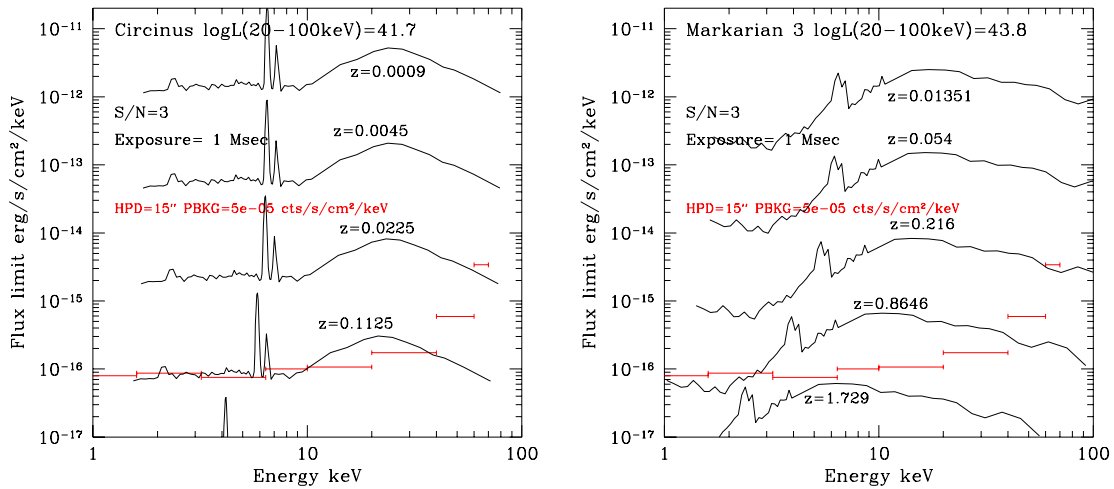


Figure 7. HEXIT-SAT flux limits compared to the redshift spectra of the Seyfert 2 galaxies Circinus Galaxy and Markarian 3. The spectra of these AGN have been measured accurately in the full 1-100 keV band by the BeppoSAX MECS and PDS instruments.

4. OUTLINING A MISSION CONCEPT: CRITICAL ISSUES ON SPACECRAFT DESIGN

Alenia Spazio performed a preliminary assessment of some aspects of the proposed experiment's satellite implementation. A 1200 kg class spacecraft is envisaged, whose service elements are drawn from the complement of ASI's standard platform PRIMA. For very low background, as proven by BeppoSAX, a circular, equatorial orbit at 600-km mean altitude is demanded. Launch into near-equatorial orbit is expected to be a standard provision of low-cost launch vehicles such as Vega, Soyuz or PSLV. Fig. 8a) shows the overall satellite configuration concept. The satellite is made up of the focal plane assembly (FPA) module and the spacecraft platform, with four embedded mirror modules, separated by an 8m long deployable boom. The satellite attitude is inertial for

the duration of at least one orbit revolution. Pointing constraints apply with respect to the sun (30 degrees), the Earth limb (30 degrees), and the Moon (5 degrees). For any pointing direction compatible with these constraints, a rotational degree of freedom, around the long axis of the spacecraft (X), is available and is used for thermal and power reasons. Initial investigations concerned the FPA thermal design and the boom design concept.

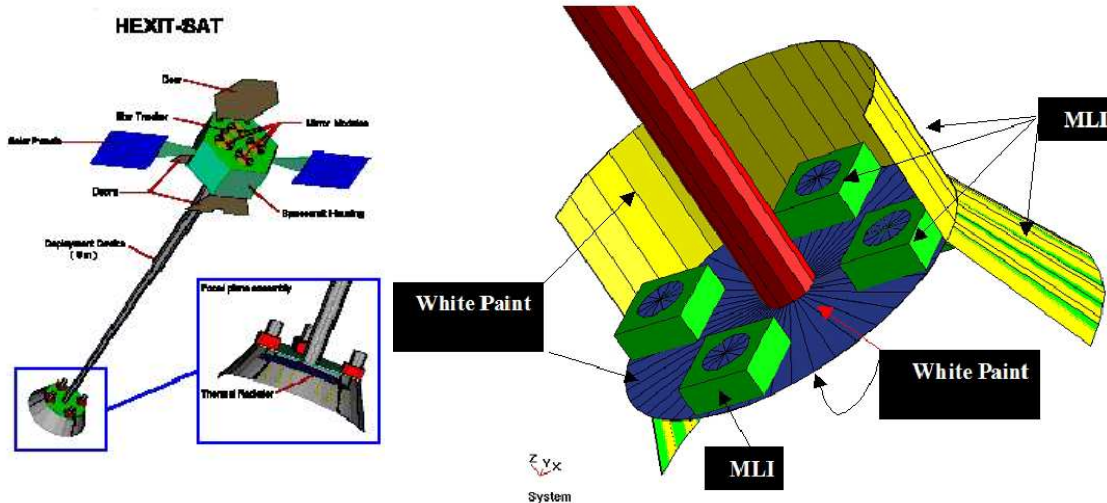


Figure 8. a), left panel: satellite Concept. The following reference frame is adopted: the Z-axis is the long axis of the boom, positive from focal plane assembly to mirror module assembly, the X-axis is the rotation axis of the solar panels, the Y-axis completes an orthonormal triad, positive in the semiplane containing the sun. b), right panel: conceptual scheme of focal plane detectors and coolers

4.1. Focal Plane Assembly thermal design

A preliminary analysis of the FPA configuration and thermal design was performed. The purpose of this exercise was to find the minimum temperature achievable in the sensors in the selected orbit and with a suitable thermal design. In the first part of the study, documented in this paper, passive approaches were addressed. The objective was to find a thermal design and configuration providing the lowest possible temperatures for the sensors, without the use of thermoelectric (Peltier) coolers. Once a configuration with suitably low base temperature is found, the addition of Peltiers will be studied.

A number of thermal design solutions were addressed. The configuration eventually selected is shown in Fig. 8b. The four detector assemblies are placed flush to a circular radiator plate, white painted on both sides. Sun shields protect the radiator from direct Sun illumination (half-cylindrical shield on the upper side, half-conical shield on the lower side). The shields are covered with multi-layer insulation (MLI) on the Sun side, and white-painted on the internal side.

The FPA temperature is affected by the Sun and Earth (albedo and IR) heat inputs, hence very sensitive to the spacecraft attitude, its orientation with respect to the Sun and the Earth. A number of different attitudes and configurations were simulated, and the selected configuration of Fig. 8b is the one that was found least affected by the environment. The coldest attitude of the S/C detector plane occurs when the satellite points at the North pole, and the Sun is in the equator plane, hence the cross section of the detector plane to the incident sunlight is very small. If no dissipation is applied, the sensor temperature is determined by Earthshine only, around -70C. This is the purely radiative equilibrium temperature for that configuration and represents the minimum obtainable temperature. Fig. 9 shows the results for a realistic case (full dissipation of 9W+9W applied to each detector, equinox, satellite pointing at 45 degrees from the equator plane), in which the effect of the Earth is considerable. The temperature of the high-energy detector (the most exposed to the environment) oscillates around -40C with small variation (+/-1C) at orbit frequency. We conclude that detector temperatures

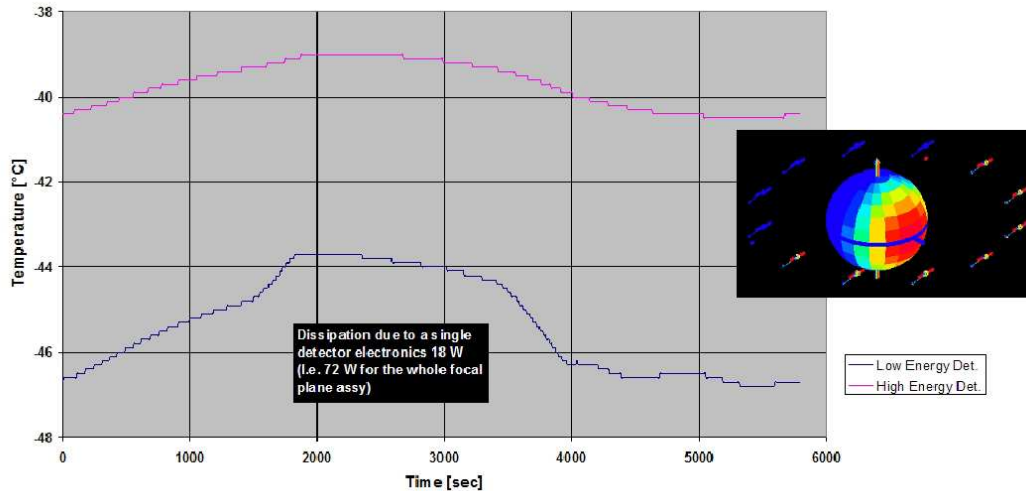


Figure 9. Detector temperature vs. Equinox, satellite pointing 45degrees from North Pole. Full detector dissipation

significantly lower than -20C (as required by one type of the low energy X-ray detector under study), at aspects to the Earth +/-30 degrees, are easily achieved by a passive thermal control approach such as that presented above.

To provide a further drop to -90C, as required by the other candidate for the low-energy detector, a thermoelectric cooler is envisaged. For the cooler to work efficiently, the dissipation applied to the sensor element must be small. A cooler applied to the detector casing is not efficient (the environmental + dissipated head load is too high). The solution involves finding a good thermal contact of the cold side of the cooler with the sensor, while the hot side has a direct thermal link (independent of that of the casing) to the radiator. The thermal contact must occur on the side of the sensor, to avoid impairing the transparency of the upper sensor to hard X-rays. For a typical Peltier, a sensor heat load of 1W and a design temperature drop of around 50 C, the power consumption of the Peltier would be less than 20W, which could be handled by the radiator. Principle solutions have been identified, and development of a prototype FPA has been proposed to test the design.

4.2. Deployable boom design

The boom must offer a reliable way of separating the FPA from the mirror modules, from an initial stowed distance of about 2 m to the operating focal length of 8 m. The driving performance requirements concern the boom dimensional stability over the time scale of an observation, under large temperature gradients (both axial and circumferential). The focal length must not change by more than 2 mm and the alignment between the optics reference axis and the focal plane reference axis must be stable within 1 arcmin. The relative position of the FPA with respect to the optics will be monitored by means of an optical alignment system. For each detected photon a positional correcting factor will be determined. Design requirements include small stowed volume, accommodation of cable harness, stiffness under launch loads by a suitable restraint system, stiffness in flight under loads from repointing and orbit maintenance maneuvers, and more. A number of design concepts were assessed, ranging from inflatable structures to telescopic booms, to coilable masts to truss-like structures. As a result of the initial investigation, two designs were selected for further study: a lightweight telescopic boom made up by seven nested cylinders, and an articulated truss structure made up of 12 bays (Fig. 10). Both structures would be made of carbon fiber for high stiffness, thermal conductivity and thermal stability. Both structure types have heritage in space missions, although the application at hand has more demanding requirements than most (loads, stability). A fully-fledged design exercise is as yet outstanding, but no feasibility problems are expected.

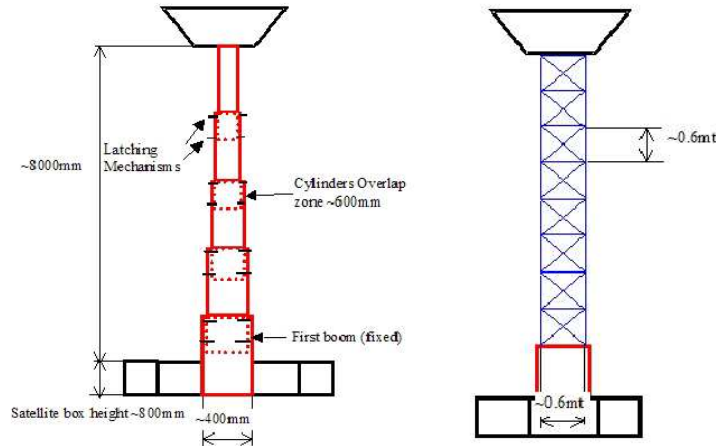


Figure 10. Two possible design for the extensible boom/truss.

ACKNOWLEDGMENTS

The original matter presented in this paper is the result of the effort of a large number of people from about ten INAF Observatories and Institutes and Italian Universities and from Alenia Spazio, which we all warmly thank.

REFERENCES

1. F. Frontera and et al. *Astron. Astroph. Suppl.* **122**, p. 357, 1997.
2. F. Ferrando and et al. *Proc. SPIE* **5168**, 2003.
3. G. Pareschi and V. Cotroneo *Proc. SPIE* **5168**, 2003.
4. H. Kunieda and et al. *Proc. SPIE* **5488**, 2004.
5. W. Craig and et al. *Proc. SPIE* **5488**, 2004.
6. K. Gebhardt and et al. *Astroph. Journal Lett.* **543**, p. L5, 2000.
7. L. Ferrarese and D. Merrit *Astroph. Journal Lett.* **539**, p. L9, 2000.
8. G. Hasinger in *The Emergence of Cosmic Structure*, S. S. Holt and C. Reynolds, eds., 2003.
9. F. Fiore and et al. *Astron. Astroph* **409**, p. 79, 2003.
10. Y. Ueda and et al. *Astroph. Journal* **598**, p. 886, 2003.
11. A. Franceschini, G. Hasinger, T. Miyaji, and D. Malguori *MNRAS* **310**, p. L5, 1999.
12. A. Comastri, G. Setti, G. Zamorani, and G. Hasinger *Astron. Astroph.* **296**, p. 1, 1995.
13. N. Menci, F. Fiore, G. C. Perola, and A. Cavaliere *Astroph. Journal* **606**, p. 58, 2004.
14. M. Worsley, A. Fabian, X. Barcons, S. Mateos, G. Hasinger, and H. Brunner *MNRAS* **in press**, 2004.
15. A. DeLuca and S. Molendi *Astron. Astroph.* **419**, p. 837, 2004.
16. A. Comastri in *Multiwavelength AGN surveys*, R. Maiolino and R. Mujica, eds., **in press**, 2004.
17. R. Fusco-Femiano and et al. *Astroph. Journal Lett.* **534**, p. L7, 2000.
18. R. Fusco-Femiano and et al. *Astroph. Journal Lett.* **602**, p. L73, 2004.
19. M. Rossetti and S. Molendi *Astron. Astroph.* **414**, p. L41, 2004.
20. K. Joensen and et al. *Appl. Opt.* **34**, p. 7935, 1995.
21. O. Citterio and et al. *Appl. Opt.* **27**, p. 1470, 1988.
22. G. Pareschi and et al. *Proc. SPIE* **5488**, 2004.
23. G. Pareschi and et al. *Proc. SPIE* **4012**, 2000.
24. S. D. Sordo and E. Caroli *Proc. SPIE* **5501**, 2004.
25. Labanti and et al. *Proc. SPIE* **4140**, p. 324, 2000.